

# Van der Waals universality near a quantum tricritical point

P. M. A. Mestrom,\* V. E. Colussi, T. Secker, G. P. Groeneveld, and S. J. J. M. F. Kokkelmans  
*Eindhoven University of Technology, P. O. Box 513, 5600 MB Eindhoven, The Netherlands*

(Dated: April 10, 2020)

We study the three-body scattering hypervolume  $D$  of atoms whose scattering length  $a$  is on the order of or smaller than the typical range  $r_{\text{vdW}}$  of the van der Waals attraction. We find that the real part of  $D$  behaves universally in this weakly interacting regime ( $|a|/r_{\text{vdW}} \lesssim 1$ ) in the absence of trimer resonances. This universality originates from hard-spherelike collisions that dominate elastic three-body scattering. We use this result to make quantitative predictions for the thermodynamics and elementary excitations of an atomic Bose-Einstein condensate in the vicinity of a quantum tricritical point, including quantum droplets stabilized by effective three-body interactions.

*Introduction.*—The thermodynamics of ultracold dilute quantum gases is determined by the asymptotic behavior of few-body scattering processes. Bosonic many-body systems can be universally described with only one parameter to characterize the two-body interactions: the  $s$ -wave scattering length  $a$  [1]. However, even in the limit  $a \rightarrow 0$  when two-body interactions effectively vanish, system properties are still determined by few-body scattering. The quantum phase diagram of a uniform Bose-Einstein condensate (BEC) in this limit is determined by the three-body scattering hypervolume  $D$  that is the analog of  $a$  [2, 3]. Provided  $\text{Re}(D) > 0$ , a quantum tricritical point exists at  $a = 0$  where the boundaries between liquid and gaseous ground states and vacuum meet [3]. Quantum tricritical points are rare, occurring for certain metallic magnets [4–6] and for a generalized Dicke model [7].

The ground-state energy density  $\mathcal{E}$  of a uniform BEC at  $a = 0$  is determined by  $D$  via

$$\mathcal{E}(n) = \frac{\hbar^2 D n^3}{6m} + \dots \quad (1)$$

where the dots indicate terms with higher powers of the number density  $n$  [2]. In the liquid phase when  $a < 0$  and  $\text{Re}(D) > 0$ , effective three-body repulsion and two-body attraction compete. This provides a three-body stabilization mechanism for liquid quantum droplets against collapse [8]. In Ref. [9], it was suggested that the experimentally observed collapse [10–13] is a relaxation process towards the liquid equilibrium state. Recently, quantum droplets were predicted [14] and experimentally observed in both mixed [15–17] and dipolar BECs [18–20], however, these systems were based on two-body stabilization mechanisms. Additionally, in typical alkali systems,  $D$  acquires an imaginary part proportional to the three-body recombination rate [21, 22], so that these states are inherently metastable. Ultimately, a quantitative understanding of droplet properties near the quantum tricritical point depends on the sign and magnitude of  $\text{Re}(D)$  for realistic systems.

For weakly interacting systems, Refs. [2, 3, 21, 23] investigated the scattering hypervolume, demonstrating how  $D$  is influenced by nonuniversal three-body quasi-bound states [21, 23] and is connected to physical observables at  $a = 0$  [3]. Nevertheless, none of these studies solved the three-body problem for two-body interaction models that contain the long-range atomic van der Waals attraction. We find that this is the essential ingredient for quantitative predictions of  $D$ , whose real part is universally fixed by the van der Waals range  $r_{\text{vdW}} = (mC_6/\hbar^2)^{1/4}/2$ , where  $C_6$  is the dispersion coefficient describing the long-range behavior of the interatomic interaction. Although the mechanisms differ, van der Waals universality also determines  $D$  in the strongly interacting regime ( $|a|/r_{\text{vdW}} \gg 1$ ) by setting the spectrum of Efimov trimers [24–35].

In this Letter, we present a numerical study of the scattering hypervolume for identical bosons interacting via pairwise van der Waals potentials in the weakly interacting regime ( $|a| \lesssim r_{\text{vdW}}$ ). We find that  $\text{Re}(D)$  is predominantly determined by  $a$  and  $r_{\text{vdW}}$  and analyze the origin of this van der Waals universality. This is used to make universal quantitative predictions for atomic BECs near the quantum tricritical point, including quantum droplets stabilized by effective three-body interactions.

*Method.*—Here we use the Alt, Grassberger, and Sandhas (AGS) approach [36] which has been proven to be a powerful method for calculating the scattering hypervolume [23]. The AGS equations,

$$U_{00}(z) = \sum_{\alpha=1}^3 T_{\alpha}(z)G_0(z)U_{\alpha 0}(z),$$

$$U_{\alpha 0}(z) = G_0^{-1}(z) + \sum_{\substack{\beta=1 \\ \beta \neq \alpha}}^3 T_{\beta}(z)G_0(z)U_{\beta 0}(z) \quad (2)$$

for  $\alpha = 1, 2, 3$ ,

are Faddeev equations for the three-body transition operators  $U_{\alpha\beta}(z)$ , where  $z$  denotes the three-body energy. The index  $\alpha(\beta)$  labels the partitions for the outgoing (incoming) state which consists of three free particles ( $\alpha = 0$ ) or a free particle and dimer ( $\alpha = 1, 2, 3$ ).  $G_0(z)$  is the free resolvent  $(z - H_0)^{-1}$ , where  $H_0$  is the three-body kinetic energy operator for the relative mo-

\*Corresponding author: p.m.a.mestrom@tue.nl

tion.  $T_\alpha(z)$  represents the two-particle transition operator for the pair  $\beta\gamma$  ( $\beta, \gamma = 1, 2, 3$ ,  $\beta \neq \gamma \neq \alpha$ ), i.e.,  $T_\alpha(z) = V_{\beta\gamma} + V_{\beta\gamma}G_0(z)T_\alpha(z)$ , where  $V_{\beta\gamma}$  is the interaction potential acting within the pair  $\beta\gamma$ . From the transition amplitude corresponding to  $U_{00}(0)$ , we determine the scattering hypervolume in the same way as described by Ref. [23] which adopts the Weinberg expansion for  $T_\alpha(z)$  [37, 38].

In the present study, we analyze the scattering hypervolume for identical bosons that interact via various van der Waals potentials, indicated by  $V_{\text{LJ}}$ ,  $V_{\text{zero}}$ ,  $V_{\text{exp}}$ , and  $V_{\text{sc}}$ . Their long-range behavior is described by the van der Waals tail  $-C_6/r^6$ , but their short-range behavior is completely different. Here  $V_{\text{LJ}}$  is the Lennard-Jones potential

$$V_{\text{LJ}} = -\frac{C_6}{r^6} \left(1 - \frac{\lambda^6}{r^6}\right), \quad (3)$$

where  $\lambda$  locates the potential barrier. The formulas for the other potentials can be found in the Supplemental Material [39]. By adjusting the potential depths, we tune the scattering length  $a$  and the number of two-body bound states [40]. We indicate the number of  $s$ -wave dimer states by adding an additional index to the potential name. For example,  $V_{\text{LJ}}^{(1)}$  supports one  $s$ -wave dimer state.

*Van der Waals universality.*—Figure 1 shows a comparison of  $D$  in the weakly interacting regime for multiple van der Waals potentials. Despite the presence of several three-body resonances,  $\text{Re}(D)$  behaves universally in contrast to  $\text{Im}(D)$ . Physically,  $\text{Im}(D)$  is determined by recombination pathways where three atoms approach at short distances, whereas  $\text{Re}(D)$  is determined through many competing pathways for elastic scattering at different length scales. When the long-range pathways dominate,  $\text{Re}(D)$  is set by the van der Waals tail and the asymptotics of the two-body scattering wave function characterized by  $r_{\text{vdW}}$  and  $a$ , respectively. We note that this picture only applies in the absence of a three-body resonance where the universality in  $\text{Re}(D)$  can be broken as shown in Fig. 1.

To identify the dominant pathway for elastic three-body scattering, we study the scaling behavior of  $\text{Re}(D)$ . In the strongly interacting regime ( $|a|/r_{\text{vdW}} \gg 1$ ), pathways that involve a single reflection from the three-body effective potentials contribute to  $D$  as  $1689 a^4$  [23, 27], both for positive and negative scattering lengths. This reflection occurs off a barrier in the three-body effective potential which acts as a hard hypersphere of hyperradius  $|a|$ . A similar result  $D = 1761.5 a^4$  is found for bosons interacting pairwise via a hard-sphere potential [2], whose repulsive character makes it inherently different from the attractive potentials considered in this Letter. However, in the weakly interacting regime ( $|a|/r_{\text{vdW}} \lesssim 1$ ), the scattering length cannot be the only length scale that determines the location of the barrier. Therefore we generalize the hard-hypersphere radius  $R_{\text{hh}}$  in the hard-hypersphere

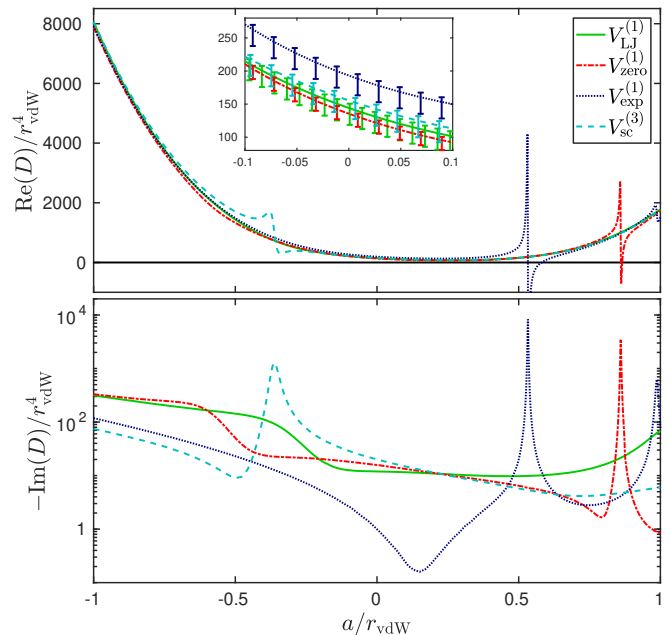


Figure 1: Three-body scattering hypervolume  $D$  corresponding to multiple van der Waals potentials as a function of the two-body scattering length  $a$  [41]. The inset shows the real part of  $D$  near the zero crossing of  $a$ .

formula,

$$\text{Re}(D) = 1689 R_{\text{hh}}^4, \quad (4)$$

to  $|a - a_{\text{hh}}^\pm|$ , where the offsets  $a_{\text{hh}}^\pm$  capture finite-range effects. We choose  $a_{\text{hh}}^\pm$  such that the hard-hypersphere formula matches the value of  $\text{Re}(D)$  at  $a/r_{\text{vdW}} = \pm 1$ . This results in the universal values  $a_{\text{hh}}^+/r_{\text{vdW}} = -0.010(3)$  and  $a_{\text{hh}}^-/r_{\text{vdW}} = 0.474(7)$  for which the uncertainties are estimated by the deviation among the considered potentials. That Eq. (4) with  $R_{\text{hh}} = |a - a_{\text{hh}}^\pm|$  describes  $\text{Re}(D)$  over a range of scattering lengths as shown in Fig. 2 confirms the dominance of hard-hyperspherelike collisions in the weakly interacting regime, except in the crossover regime  $-0.1 \lesssim a/r_{\text{vdW}} \lesssim 0.6$ .

As long as  $R_{\text{hh}} > \lambda$ , where  $\lambda$  is a characteristic length scale of the short-range details of the interaction potential, one can expect that  $R_{\text{hh}}$  is set by  $a$  and  $r_{\text{vdW}}$ . Figure 2 shows that the regime where  $|a - a_{\text{hh}}^\pm|$  does not describe  $R_{\text{hh}}$  is roughly determined by  $R_{\text{hh}} \lesssim \lambda$ . In the limit of deep van der Waals potentials,  $\lambda/r_{\text{vdW}}$  approaches zero. This implies that the  $-C_6/r^6$  behavior is approached at smaller values of  $r/r_{\text{vdW}}$ . Therefore, we expect that  $\text{Re}(D)$  of deep van der Waals potentials behaves universally in the complete weakly interacting regime in the absence of trimer resonances [42].

For a Lennard-Jones potential supporting no two-body bound states ( $V_{\text{LJ}}^{(0)}$ ), we find  $D/r_{\text{vdW}}^4 = 86 \pm 2$  at  $a = 0$  and compare this result to the value 90 predicted by Zwinger [3, 39, 43]. This prediction is based upon an earlier many-body calculation for the energy per particle of a

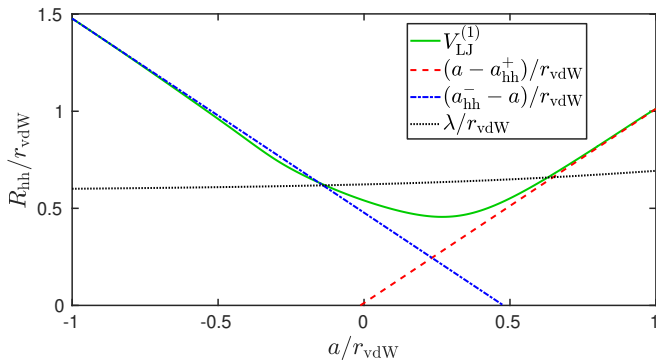


Figure 2: The hard-sphere radius  $R_{\text{hh}} = [\text{Re}(D)/1689]^{1/4}$  corresponding to the potential  $V_{\text{LJ}}^{(1)}$  (green solid line) as a function of the two-body scattering length  $a$ . The dashed and dash-dotted curves show  $(a - a_{\text{hh}}^+)/r_{\text{vdW}}$  and  $(a_{\text{hh}}^- - a)/r_{\text{vdW}}$ , respectively, for which  $a_{\text{hh}}^{\pm}$  is modified to match  $\text{Re}(D)$  at  $a/r_{\text{vdW}} = \pm 1$ . The values of  $a_{\text{hh}}^+/r_{\text{vdW}}$  and  $a_{\text{hh}}^-/r_{\text{vdW}}$  are  $-0.012$  and  $0.477$ , respectively. The dotted curve displays the position  $\lambda/r_{\text{vdW}}$  of the repulsive barrier of  $V_{\text{LJ}}^{(1)}$ . Note that  $R_{\text{hh}}$  is slightly affected by a trimer resonance near  $a/r_{\text{vdW}} \simeq -0.3$  [39].

Bose fluid at zero temperature and zero pressure near the quantum tricritical point [44]. This close agreement demonstrates that  $D$  can be determined from properties of ultracold Bose systems near the quantum tricritical point, which we turn to presently.

*Thermodynamics and elementary excitations.*—How does the scattering hypervolume determine the ground-state properties and excitations of a BEC near the quantum tricritical point? To understand these effects, we follow Ref. [3] and study the effective Lagrangian density valid at weak interactions and zero temperature

$$\mathcal{L} = \frac{i\hbar}{2} [\Psi^* \dot{\Psi} - \Psi \dot{\Psi}^*] - \frac{\hbar^2}{2m} |\nabla \Psi|^2 - V_{\text{ext}}(\mathbf{r}) |\Psi|^2 - \frac{2\pi\hbar^2 a}{m} |\Psi|^4 - \frac{\hbar^2 D}{6m} |\Psi|^6. \quad (5)$$

The Gross-Pitaevskii equation follows from minimizing the action  $S = \int d^3r dt \mathcal{L}$ , giving

$$i\hbar \dot{\Psi} = -\frac{\hbar^2}{2m} \nabla^2 \Psi + V_{\text{ext}}(\mathbf{r}) \Psi + \frac{4\pi\hbar^2 a}{m} |\Psi|^2 \Psi + \frac{\hbar^2 D}{2m} |\Psi|^4 \Psi. \quad (6)$$

The condensate wave function is formulated as  $\Psi(\mathbf{r}, t) = \sqrt{n(\mathbf{r}, t)} e^{-i\phi(\mathbf{r}, t)}$  satisfying the Josephson relation  $\hbar \dot{\phi} = -\mu$  under stationary conditions. In Eq. (6), higher-order effects have been ignored as well as the energy dependence of the few-body scattering amplitudes [45–47]. In the following, we focus on signatures of  $D$  in uniform and trapped systems with  $V_{\text{ext}}(\mathbf{r}) = m\omega_{\text{ho}}^2(\lambda_x^2 x^2 + \lambda_y^2 y^2 + \lambda_z^2 z^2)/2$ . We define the oscillator length  $l_{\text{ho}} = \sqrt{\hbar/m\omega_{\text{ho}}}$  and the geometric means  $\bar{\omega} = \omega_{\text{ho}}(\lambda_x \lambda_y \lambda_z)^{1/3}$  and  $\bar{l} = \sqrt{\hbar/m\bar{\omega}}$ . In this analysis, we neglect the imaginary part of  $D$  since our results for  $V_{\text{LJ}}^{(1)}$  show that  $|\text{Re}(D)/\text{Im}(D)|$

varies from roughly 10 near  $a = 0$  to roughly 25 near  $a/r_{\text{vdW}} = \pm 1$ , and we return to this point below when discussing the experimental outlook.

At the point  $a = 0$ , where we estimate  $\text{Re}(D)/r_{\text{vdW}}^4 \approx 100$ , Eqs. (5) and (6) contain only effective three-body interactions. This regime for a uniform gas was considered in Ref. [3], finding chemical potential  $\mu = D\hbar^2 n^2/2m$ , pressure  $P = (8m/9D\hbar^2)^{1/2} \mu^{3/2}$  and sound velocity  $c = \hbar n \sqrt{D}/m$ . For the ground state of a trapped gas, the Thomas-Fermi approximation gives  $n(\mathbf{r}) = (2m[\mu - V_{\text{ext}}(\mathbf{r})]/D\hbar^2)^{1/2}$ . After normalization, the chemical potential is fixed to  $\mu/\hbar\bar{\omega} = \zeta^{1/4}/\pi$  in terms of the three-body Thomas-Fermi parameter  $\zeta = DN^2/\bar{l}^4$ . Likewise, integrating the thermodynamic relation  $\mu = \partial_N E$  gives energy per particle  $E/N = 2\mu/3$ , from which we infer the interaction energy per particle  $E_{\text{int}}/N = \mu/6$  as a consequence of the virial theorem [48]. At the cloud boundaries  $\mu = m\omega_{\text{ho}}^2 \lambda_\eta^2 R_\eta^2/2$  ( $\eta = x, y, z$ ), and we estimate the spatial extent of the cloud from the geometric mean of the semi-axes  $\bar{R} \equiv (R_x R_y R_z)^{1/3} = \sqrt{2/\pi} \bar{l} \zeta^{1/8}$ . Compared to the Thomas-Fermi limit for two-body interactions, we find that a smaller portion of the total energy is involved in interactions, however, due to the  $N^2$  scaling of  $\zeta$ , all energies and radii scale with higher powers of  $N$ .

To investigate the shift of discretized collective modes in a harmonic trap at  $a = 0$ , we use a time-dependent trial wave function [49–51]

$$\Psi(x, y, z, t) = A(t) \prod_{\eta=x,y,z} e^{-\frac{(\eta-\eta_0)^2}{2w_\eta^2} + i\eta\alpha_\eta + i\eta^2\beta_\eta}, \quad (7)$$

with time-dependent variational parameters  $\{w_\eta, \eta_0, \alpha_\eta, \beta_\eta\}_{\eta=x,y,z}$ . The magnitude of  $A$  is set by particle number conservation. Minimizing the action with respect to the variational parameters, we find

$$\partial_\tau^2 \eta_0 + \lambda_\eta^2 \eta_0 = 0, \quad (8)$$

$$\partial_\tau^2 v_\eta + \lambda_\eta^2 v_\eta = \frac{1}{v_\eta^3} + \frac{K}{v_\eta(v_x v_y v_z)^2} \quad (\eta = x, y, z), \quad (9)$$

with  $K = 2DN^2/9\sqrt{3}\pi^3 l_{\text{ho}}^4$  and dimensionless scalings  $v_\eta = w_\eta/l_{\text{ho}}$  and  $\tau = \omega_{\text{ho}} t$ . Equation (8) describes dipole oscillations of the condensate center with trap frequencies in agreement with the Kohn theorem [52]. Linearizing Eq. (9) about equilibrium, yields mode frequencies  $\omega_{022}$ ,  $\omega_{100}$ , and  $\omega_{020}$  in terms of principle and angular quantum numbers parametrized as  $\omega_{nlm}$  [49] (see Ref. [39]). Our results for these modes at  $a = 0$  are shown in Figs. 3(a)–3(d) over a range of geometries and values of  $K$  compared against results in the noninteracting and Thomas-Fermi limits. Experimentally,  $D$  can be inferred from frequency shifts intermediate to these limits. From Fig. 3(d), this contrast is maximized for the breathing mode  $\omega_{100}$  in an isotropic geometry. In the Thomas-Fermi limit, this mode shifts to  $2\sqrt{2}\omega_{\text{ho}}$ , which is beyond the result  $\sqrt{5}\omega_{\text{ho}}$  for two-body interactions [53]. Physically, the simultaneous compression of this mode along all axes leads to increased densities near trap center and the largest non-linear interaction effects [54].

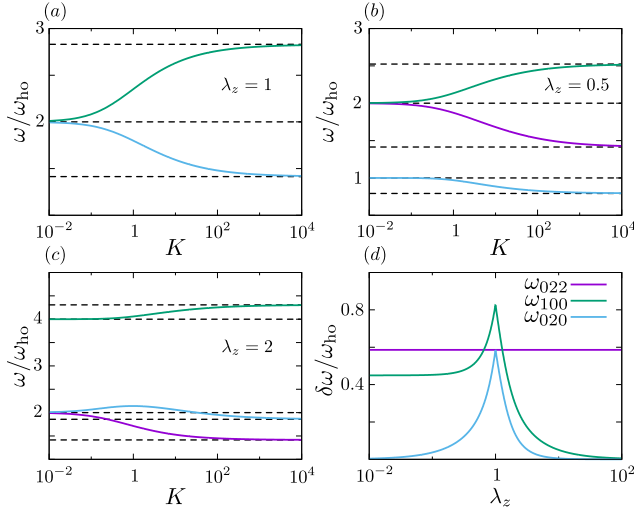


Figure 3: Collective mode frequencies at  $a = 0$  versus  $K = 2DN^2/9\sqrt{3}\pi^3 t_{\text{ho}}^4$  for (a) isotropic, (b) cigar, and (c) pancake geometries. We set  $\lambda_x = \lambda_y = 1$  and vary  $\lambda_z$ . The  $\omega_{020}$  and  $\omega_{022}$  modes are degenerate for an isotropic trap. Dashed lines indicate results in the noninteracting and Thomas-Fermi limits. (d) Contrast  $\delta\omega_{nlm} \equiv \omega_{nlm}|_{K \gg 1} - \omega_{nlm}|_{K=0}$  versus trap aspect ratio  $\lambda_z$ .

For  $a < 0$ , it is possible that  $D > 0$  can stabilize the BEC against collapse. Taking the Gaussian trial wave function of Eq. (7) with  $\eta_0 = \alpha_\eta = \beta_\eta = 0$  and  $w_\eta = w$ , we minimize the energy

$$E = \frac{3\hbar^2 N}{4m w^2} + \frac{\hbar^2 a}{\sqrt{2\pi m}} \frac{N^2}{w^3} + \frac{\hbar^2 D}{18\sqrt{3}\pi^3 m} \frac{N^3}{w^6} \quad (10)$$

in the absence of a trapping potential for a fixed number of particles  $N$ . We find that no droplets exist for  $N \leq N_c$  where

$$N_c = \frac{2^{7/2}}{3^{11/4}\sqrt{\pi}} \frac{\sqrt{D}}{a^2}. \quad (11)$$

The droplets are metastable for  $N_c < N \leq 3\sqrt{3}N_c/4 = N_s$  and stable for  $N > N_s$ . The variational dependence of the energy as a function of the width  $w$  is illustrated in Fig. 4(a) for the unstable, metastable, and stable regimes. The density profiles of the droplets numerically obtained from Eq. (6) are depicted in Fig. 4(b) for various  $N$  which shows that the Gaussian trial wave function is reasonable near the metastable regime. Figure 4(c) shows the phase diagram of the Bose fluid for  $a < 0$  using Eq. (4) with  $R_{\text{hh}} = |a - 0.477 r_{\text{vdW}}|$  while neglecting  $\text{Im}(D)$ . For large  $N$  the density profile is almost constant with density  $n_0 = 6\pi|a|/D$  [8] which is approximately a factor 2.18 larger than the center density of a droplet with  $N = N_c$ . In the large  $N$  limit, the Gaussian trial wave function overestimates the center density by roughly a factor 1.84. Previous estimates of  $n_0$  in Ref. [9] are larger by roughly a factor of 5 to 10 than our result, which we attribute to an underestimation of effective three-body repulsion in that work.

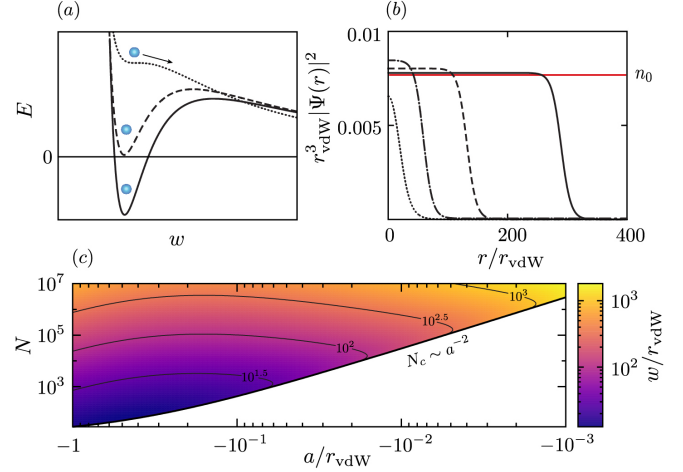


Figure 4: Ground-state properties of Bose droplets. (a) Illustrated dependence of the energy  $E$  given by Eq. (10) with width  $w$  for  $N > N_s$  (solid),  $N = N_s$  (dashed), and  $N = N_c$  (dotted). (b) Numerical ground-state profile versus radial coordinate for  $N/N_s \approx 1$  (dotted), 10 (dash-dotted), 100 (dashed), and 1000 (solid) evaluated at  $a = -0.08 r_{\text{vdW}}$  taking our result for  $V_{\text{LJ}}^{(1)}$ ,  $\text{Re}(D) = 197 r_{\text{vdW}}^4$  (see Fig. 1 inset), compared with the large- $N$  density  $n_0$  indicated by the solid red curve. (c) Droplet width  $w$  versus  $a$  and  $N$  from the Gaussian trial wave function Eq. (7) using Eq. (4) with  $R_{\text{hh}} = |a - 0.477 r_{\text{vdW}}|$  and neglecting  $\text{Im}(D)$ . The liquid-to-gas transition at  $N_c$  is indicated by the solid line.

*Experimental outlook.*—Let us now discuss the experimental possibilities to observe the effects of  $D$ . For this purpose, we take  $\text{Im}(D)$  into account in the typical lifetime  $\tau_{\text{life}} = 1/L_3 n^2$  where  $L_3 = -\text{Im}(D)\hbar/m$  determines the loss rate of atoms from the BEC via three-body recombination [21]. For quantum droplets with density  $n_0$  and chemical potential  $\mu_0 = -6\pi^2\hbar^2 a^2/m\text{Re}(D)$  [8], we compare  $\tau_{\text{life}}$  to the characteristic timescale  $\tau_0 = \hbar/|\mu_0|$  and find  $\tau_{\text{life}}/\tau_0 = -\text{Re}(D)/6\text{Im}(D)$ , which is typically larger than one according to our results for  $D$ . Since  $\tau_{\text{life}} \propto [\text{Re}(D)]^2/\text{Im}(D)a^2$ , longer lifetimes can be achieved at smaller  $|a|$ . However, the critical number  $N_c$  also increases in this limit [see Fig. 4(c)].

To observe the collective mode frequencies at  $a = 0$ , we require  $\tau_{\text{life}} > \tau_{\text{ho}} = 2\pi/\omega_{\text{ho}}$ . In the Thomas-Fermi limit, we find

$$\frac{\tau_{\text{life}}}{\tau_{\text{ho}}} = \frac{\text{Re}(D)}{\text{Im}(D)} \frac{1}{2 \cdot 3^{5/8} (2\pi)^{3/4} \lambda_z^{1/2} K^{1/4}} \quad (12)$$

for cylindrically symmetric traps with  $\lambda_x = \lambda_y = 1$  using the center density to estimate  $\tau_{\text{life}}$ . In general, smaller  $\lambda_z$  is advantageous for achieving large  $K$  for fixed  $\tau_{\text{life}}/\tau_{\text{ho}}$  and  $D$ . Figure 3(d) shows that  $\delta\omega_{022}/\omega_{\text{ho}}$  and  $\delta\omega_{100}/\omega_{\text{ho}}$  are roughly 0.5 for small  $\lambda_z$  which makes these modes suitable for extracting  $\text{Re}(D)$  from the  $K$  dependence of the corresponding mode frequencies. Cigar-shaped traps can also be used to measure the speed of sound at  $a = 0$  provided that the characteristic distance  $c\tau_{\text{life}}$  is large

enough to resolve experimentally. Using our previous estimate for  $\tau_{\text{life}}$  in the Thomas-Fermi limit, we find

$$c\tau_{\text{life}} = -\sqrt{\frac{\pi}{2}} \frac{[\text{Re}(D)]^{5/4} \sqrt{N}}{\text{Im}(D) \zeta^{3/8}}, \quad (13)$$

which scales as  $\lambda_z^{-1/4}$ .

*Conclusion.*—We study the scattering hypervolume  $D$  for identical bosons interacting via pairwise van der Waals potentials. Our results show that  $\text{Re}(D)$  is predominantly determined by the long-range two-body properties  $r_{\text{vdW}}$  and  $a$ . The van der Waals universality of this behavior is due to dominant hard-hypersphere scattering. However,  $\text{Im}(D)$  depends strongly on the short-range details of the interaction, resulting in nonuniversal behavior. In the limit of vanishing  $a$ ,  $\text{Re}(D)$  determines the quantum phase diagram near the tricritical point. Using the van der Waals universality of  $\text{Re}(D)$ , we make quan-

titative predictions for the properties of atomic BECs, including the formation of quantum droplets.

Further studies of  $D$  for deeper van der Waals potentials need to be conducted to test the robustness of the universal behavior in  $\text{Re}(D)$  in the weakly interacting regime. The influence of multichannel physics on  $D$  could lead to new interesting phenomena at small scattering lengths due to additional parameters characterizing the zero crossing of  $a$  [55–57]. Dynamical studies including effective three-body repulsion are needed to understand droplet formation.

*Acknowledgements.*—We thank Wilhelm Zwerger, Jinglun Li, Silvia Musolino, and Denise Ahmed-Braun for fruitful discussions. This research is financially supported by the Netherlands Organisation for Scientific Research (NWO) under Grant No. 680-47-623 and by the Foundation for Fundamental Research on Matter (FOM).

- 
- [1] K. Huang, *Statistical Mechanics* (Wiley, New York, 1963).
- [2] S. Tan, Phys. Rev. A **78**, 013636 (2008).
- [3] W. Zwerger, Journal of Statistical Mechanics: Theory and Experiment **2019**, 103104 (2019).
- [4] D. Belitz and T. R. Kirkpatrick, Phys. Rev. Lett. **119**, 267202 (2017).
- [5] S. Friedemann, W. J. Duncan, M. Hirschberger, T. W. Bauer, R. Küchler, A. Neubauer, M. Brando, C. Pfleiderer, and F. M. Grosche, Nature Physics **14**, 62 (2018).
- [6] U. S. Kaluarachchi, V. Taufour, S. L. Bud'ko, and P. C. Canfield, Phys. Rev. B **97**, 045139 (2018).
- [7] Y. Xu and H. Pu, Phys. Rev. Lett. **122**, 193201 (2019).
- [8] A. Bulgac, Phys. Rev. Lett. **89**, 050402 (2002).
- [9] B. Gao, Journal of Physics B: Atomic, Molecular and Optical Physics **37**, L227 (2004).
- [10] J. M. Gerton, D. Strekalov, I. Prodan, and R. G. Hulet, Nature **408**, 692 (2000).
- [11] J. L. Roberts, N. R. Claussen, S. L. Cornish, E. A. Donley, E. A. Cornell, and C. E. Wieman, Phys. Rev. Lett. **86**, 4211 (2001).
- [12] E. A. Donley, N. R. Claussen, S. L. Cornish, J. L. Roberts, E. A. Cornell, and C. E. Wieman, Nature **412**, 295 (2001).
- [13] C. Eigen, A. L. Gaunt, A. Suleymanzade, N. Navon, Z. Hadzibabic, and R. P. Smith, Phys. Rev. X **6**, 041058 (2016).
- [14] D. S. Petrov, Phys. Rev. Lett. **115**, 155302 (2015).
- [15] C. R. Cabrera, L. Tanzi, J. Sanz, B. Naylor, P. Thomas, P. Cheiney, and L. Tarruell, Science **359**, 301 (2018).
- [16] P. Cheiney, C. R. Cabrera, J. Sanz, B. Naylor, L. Tanzi, and L. Tarruell, Phys. Rev. Lett. **120**, 135301 (2018).
- [17] G. Semeghini, G. Ferioli, L. Masi, C. Mazzinghi, L. Wolswijk, F. Minardi, M. Modugno, G. Modugno, M. Inguscio, and M. Fattori, Phys. Rev. Lett. **120**, 235301 (2018).
- [18] H. Kadau, M. Schmitt, M. Wenzel, C. Wink, T. Maier, I. Ferrier-Barbut, and T. Pfau, Nature **530**, 194 (2016).
- [19] I. Ferrier-Barbut, H. Kadau, M. Schmitt, M. Wenzel, and T. Pfau, Phys. Rev. Lett. **116**, 215301 (2016).
- [20] L. Chomaz, S. Baier, D. Petter, M. J. Mark, F. Wächtler, L. Santos, and F. Ferlaino, Phys. Rev. X **6**, 041039 (2016).
- [21] S. Zhu and S. Tan, arXiv:1710.04147v1 [cond-mat.quant-gas] (2017).
- [22] E. Braaten and H.-W. Hammer, Phys. Rep. **428**, 259 (2006).
- [23] P. M. A. Mestrom, V. E. Colussi, T. Secker, and S. J. J. M. F. Kokkelmans, Phys. Rev. A **100**, 050702(R) (2019).
- [24] M. Berninger, A. Zenesini, B. Huang, W. Harm, H.-C. Nägerl, F. Ferlaino, R. Grimm, P. S. Julienne, and J. M. Hutson, Phys. Rev. Lett. **107**, 120401 (2011).
- [25] P. Naidon and S. Endo, Rep. Prog. Phys. **80**, 056001 (2017).
- [26] C. H. Greene, P. Giannakeas, and J. Pérez-Ríos, Rev. Mod. Phys. **89**, 035006 (2017).
- [27] J. P. D’Incao, Journal of Physics B: Atomic, Molecular and Optical Physics **51**, 043001 (2018).
- [28] J. Wang, J. P. D’Incao, B. D. Esry, and C. H. Greene, Phys. Rev. Lett. **108**, 263001 (2012).
- [29] Y. Wang, J. Wang, J. P. D’Incao, and C. H. Greene, Phys. Rev. Lett. **109**, 243201 (2012).
- [30] R. Schmidt, S. Rath, and W. Zwerger, The European Physical Journal B **85**, 386 (2012).
- [31] P. Naidon, S. Endo, and M. Ueda, Phys. Rev. A **90**, 022106 (2014).
- [32] D. Blume, Few-Body Systems **56**, 859 (2015).
- [33] P. Naidon, E. Hiyama, and M. Ueda, Phys. Rev. A **86**, 012502 (2012).
- [34] P. K. Sørensen, D. V. Fedorov, A. S. Jensen, and N. T. Zinner, Phys. Rev. A **88**, 042518 (2013).
- [35] R. Chapurin, X. Xie, M. J. Van de Graaff, J. S. Popowski, J. P. D’Incao, P. S. Julienne, J. Ye, and E. A. Cornell, Phys. Rev. Lett. **123**, 233402 (2019).
- [36] E. Alt, P. Grassberger, and W. Sandhas, Nucl. Phys. B **2**, 167 (1967).
- [37] S. Weinberg, Phys. Rev. **131**, 440 (1963).
- [38] P. M. A. Mestrom, T. Secker, R. M. Kroeze, and S. J. J. M. F. Kokkelmans, Phys. Rev. A **99**, 012702 (2019).
- [39] See Supplemental Material for additional details of our calculations and results.

- [40] The scattering length contains a resonant and nonresonant contribution. The latter is known as the background scattering length and is on the order of  $r_{\text{vdW}}$  for the considered van der Waals potentials.
- [41] There could be additional narrow trimer resonances for which our grid for  $a$  is too sparse. Such resonances would have a width smaller than  $\delta a = 10^{-3} r_{\text{vdW}}$ .
- [42] This expectation is consistent with our results of  $\text{Re}(D)$  for the potentials  $V_{\text{sc}}^{(1)}$ ,  $V_{\text{sc}}^{(2)}$  and  $V_{\text{sc}}^{(3)}$  which approach the universal curve as the potential depth increases [39].
- [43] The uncertainty in this prediction is determined by the validity of the approximations that are made in Ref. [44], including the trial wave function that is used to describe the ground state of the Bose fluid near the quantum tricritical point.
- [44] M. D. Miller, L. H. Nosanow, and L. J. Parish, Phys. Rev. B **15**, 214 (1977).
- [45] H. Fu, Y. Wang, and B. Gao, Phys. Rev. A **67**, 053612 (2003).
- [46] A. Collin, P. Massignan, and C. J. Pethick, Phys. Rev. A **75**, 013615 (2007).
- [47] M. Thøgersen, N. T. Zinner, and A. S. Jensen, Phys. Rev. A **80**, 043625 (2009).
- [48] F. Dalfovo, S. Giorgini, L. P. Pitaevskii, and S. Stringari, Rev. Mod. Phys. **71**, 463 (1999).
- [49] V. M. Pérez-García, H. Michinel, J. I. Cirac, M. Lewenstein, and P. Zoller, Phys. Rev. Lett. **77**, 5320 (1996).
- [50] S. Yi and L. You, Phys. Rev. A **63**, 053607 (2001).
- [51] H. Al-Jibbouri, I. Vidanović, A. Balaž, and A. Pelster, Journal of Physics B: Atomic, Molecular and Optical Physics **46**, 065303 (2013).
- [52] W. Kohn, Phys. Rev. **123**, 1242 (1961).
- [53] S. Stringari, Phys. Rev. Lett. **77**, 2360 (1996).
- [54] C. J. E. Straatsma, V. E. Colussi, M. J. Davis, D. S. Lobsenz, M. J. Holland, D. Z. Anderson, H. J. Lewandowski, and E. A. Cornell, Phys. Rev. A **94**, 043640 (2016).
- [55] Z. Shotan, O. Machtey, S. Kokkelmans, and L. Khaykovich, Phys. Rev. Lett. **113**, 053202 (2014).
- [56] A. Pricoupenko and D. S. Petrov, Phys. Rev. A **100**, 042707 (2019).
- [57] C. Chin, R. Grimm, P. Julienne, and E. Tiesinga, Rev. Mod. Phys. **82**, 1225 (2010).

# Supplemental Material: “Van der Waals universality near a quantum tricritical point”

P. M. A. Mestrom,<sup>1</sup> V. E. Colussi,<sup>1</sup> T. Secker,<sup>1</sup> G. P. Groeneveld,<sup>1</sup> and S. J. J. M. F. Kokkelmans<sup>1</sup>

<sup>1</sup>*Eindhoven University of Technology, P. O. Box 513, 5600 MB Eindhoven, The Netherlands*

## I. TWO-BODY INTERACTION MODELS

In this work, we have analyzed the behavior of the scattering hypervolume using the following interaction potentials to mimic interatomic interactions:

$$V_{\text{LJ}} = -\frac{C_6}{r^6} \left( 1 - \frac{\lambda^6}{r^6} \right), \quad (\text{S1})$$

$$V_{\text{zero}} = -\frac{C_6}{r^6} \Theta(r - \lambda), \quad (\text{S2})$$

$$V_{\text{exp}} = -\frac{C_6}{r^6} \exp(-\lambda^6/r^6), \quad (\text{S3})$$

$$V_{\text{sc}} = -\frac{C_6}{r^6 + \lambda^6}. \quad (\text{S4})$$

These potentials are displayed in Fig. S1. They are all dominated by the van der Waals interaction,  $-C_6/r^6$ , for large interparticle separations  $r$  (i.e.,  $r \gg \lambda$ ). The potential in Eq. (S1) is known as the Lennard-Jones potential. It is strongly repulsive for  $r < \lambda$ . To handle the infinitely strong repulsive barrier numerically, we cut off this barrier as follows:

$$V(r) = \begin{cases} -\frac{C_6}{r_0^6} \left( 1 - \frac{\lambda^6}{r_0^6} \right), & 0 \leq r < r_0, \\ -\frac{C_6}{r^6} \left( 1 - \frac{\lambda^6}{r^6} \right), & r \geq r_0. \end{cases} \quad (\text{S5})$$

We choose  $r_0$  small enough such that the height of the barrier is much larger than the depth of the well. In Eq. (S2),  $\Theta(x)$  is the Heaviside step function. It is zero for  $x < 0$  and 1 for  $x \geq 0$ . This potential is thus zero for  $r < \lambda$  and consists of a pure van der Waals tail for  $r \geq \lambda$ . The potential  $V_{\text{exp}}$  defined in Eq. (S3) also goes to zero for  $r \rightarrow 0$ , but in a smooth way. Finally, Eq. (S4) represents a van der Waals potential with a “soft core”. It is attractive for all values of  $r$ .

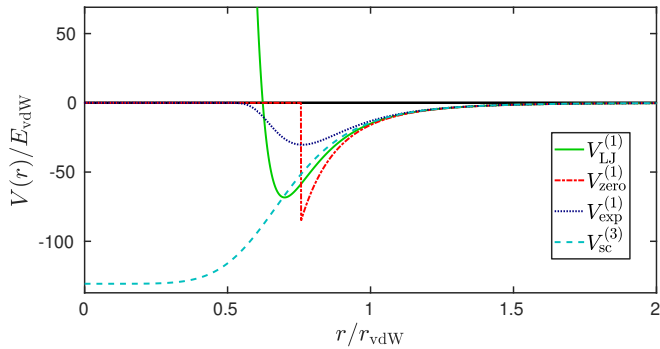


Figure S1: The considered van der Waals potentials in units of  $E_{\text{vdW}} \equiv \hbar^2/(mr_{\text{vdW}}^2)$  as a function of the interparticle distance  $r$ . The potential depths are chosen such that  $a = 0$ .

## II. THREE-BODY RESONANCES

In the weakly interacting regime, the scattering hypervolume is influenced by nonuniversal trimer resonances [21, 23]. Figure 1 of the main text shows several of such trimer resonances. Some resonances have only a weak effect on  $D$ . For example, the Lennard-Jones potential  $V_{\text{LJ}}^{(1)}$  supports a three-body quasibound state at zero energy near  $a/r_{\text{vdW}} \simeq -0.3$ . Figure S2 shows that this trimer resonance vanishes when the two-body  $g$ -wave state that gets bound at  $a/r_{\text{vdW}} = -4.8$  is removed from the Weinberg expansion of the two-body interaction potential  $V$ . This demonstrates its strong  $g$ -wave character.

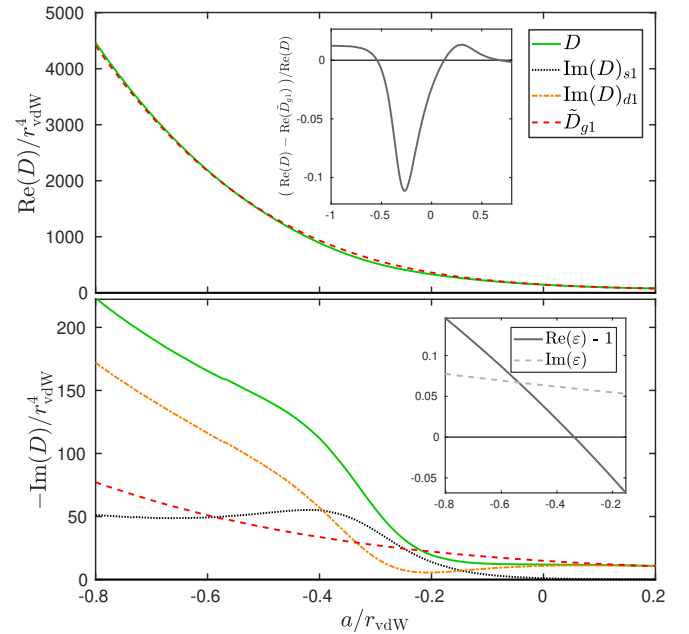


Figure S2: Three-body scattering hypervolume  $D$  corresponding to the Lennard-Jones potential  $V_{\text{LJ}}^{(1)}$  as a function of the two-body scattering length  $a$ . Its imaginary part can be written as  $\text{Im}(D) = \text{Im}(D)_{s1} + \text{Im}(D)_{d1}$ , where  $\text{Im}(D)_{s1}$  and  $\text{Im}(D)_{d1}$  are proportional to the partial three-body recombination rates into the first  $s$ -wave and  $d$ -wave dimer state, respectively. Additionally,  $\tilde{D}_{g1}$  is the scattering hypervolume obtained by excluding the first  $g$ -wave term of the Weinberg expansion. The upper inset shows the relative difference between the real parts of  $D$  and  $\tilde{D}_{g1}$ . The lower inset shows the behavior of the eigenvalue  $\epsilon$  of the kernel of the three-body integral equation causing this trimer resonance. Near the resonance position, the real part of  $\epsilon$  passes one as discussed in Ref. [38].

### III. ADDITIONAL RESULTS FOR THE SOFT-CORE VAN DER WAALS POTENTIAL

We have calculated the three-body scattering hypervolume  $D$  in the weakly interacting regime corresponding to the soft-core van der Waals potential supporting one, two and three  $s$ -wave dimer states. These results are presented in Fig. S3. This figure shows that the real part of  $D$  in the weakly interacting regime for  $V_{\text{sc}}^{(1)}$  and  $V_{\text{sc}}^{(2)}$  is strongly influenced by trimer resonances and deviates strongly from  $\text{Re}(D)$  for  $V_{\text{sc}}^{(3)}$ . Therefore, we conclude that the potentials  $V_{\text{sc}}^{(1)}$  and  $V_{\text{sc}}^{(2)}$  are too shallow to obey the van der Waals universality in  $\text{Re}(D)$ . Furthermore, we find a sharp minimum in  $-\text{Im}(D)$  for  $V_{\text{sc}}^{(1)}$  at  $a/r_{\text{vdW}} = 0.739$  which is likely to be caused by destructive interference between competing pathways for three-body recombination [27].

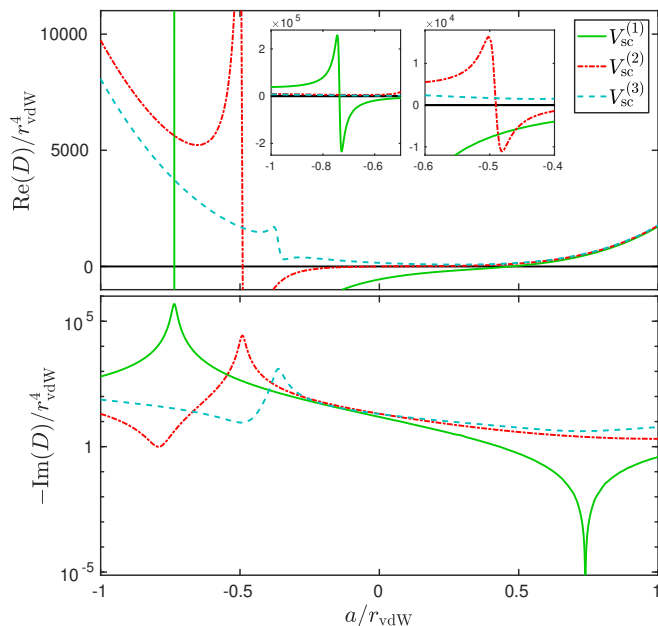


Figure S3: Three-body scattering hypervolume  $D$  corresponding to soft-core van der Waals potentials supporting one, two and three  $s$ -wave dimer states as a function of the two-body scattering length  $a$ . The insets display some trimer resonances.

### IV. ADDITIONAL RESULTS FOR THE SQUARE-WELL POTENTIAL

In this section we consider identical bosons interacting via pairwise square-well potentials defined by

$$V_{\text{sw}}(r) = \begin{cases} -V_0, & 0 \leq r < R, \\ 0, & r \geq R. \end{cases} \quad (\text{S6})$$

Here  $R$  and  $V_0$  represent the range and depth of the potential, respectively. We have calculated the three-

body scattering hypervolume  $D$  in the weakly interacting regime corresponding to the square-well potential supporting one, two and three  $s$ -wave dimer states. Parts of these results have been presented in Ref. [23]. Figure S4 shows the results as a function of the two-body scattering length  $a$ . Clearly, the real part of  $D$  still follows the universal  $a^4$  scaling for  $a/R \gtrsim 0.7$ . However, this universality vanishes as  $a$  decreases.

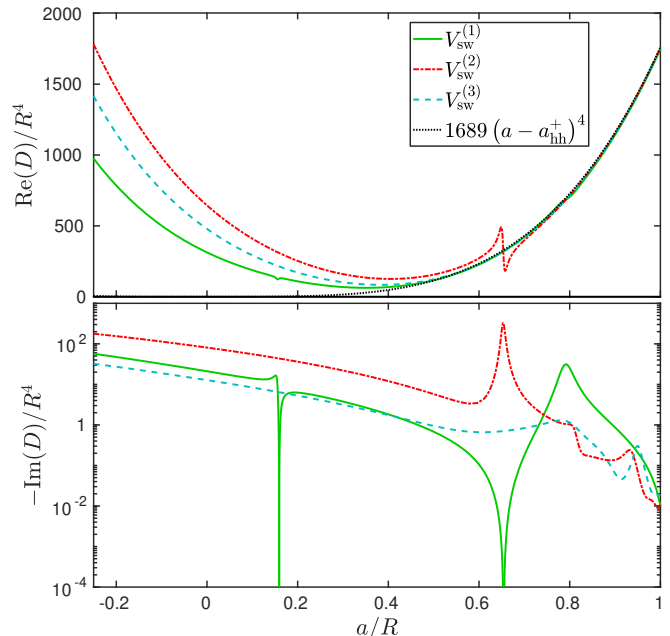


Figure S4: Three-body scattering hypervolume  $D$  corresponding to square-well potentials supporting one, two and three  $s$ -wave dimer states as a function of the two-body scattering length  $a$ . We have presented the results for  $V_{\text{sw}}^{(1)}$  and  $V_{\text{sw}}^{(2)}$  before in Ref. [23]. The black dotted line corresponds to the curve  $D = 1689(a - a_{\text{hh}}^+)^4$  where  $a_{\text{hh}}^+/R = -0.01$ . The choice of this value is based on the values of  $D$  for  $V_{\text{sw}}^{(1)}$ ,  $V_{\text{sw}}^{(2)}$  and  $V_{\text{sw}}^{(3)}$  at  $a/R = 1$ .

### V. ZWERGER'S PREDICTION

Here we consider a Bose fluid at zero temperature and zero pressure. The bosons interact via a pairwise Lennard-Jones potential (see Eq. (S1)) that supports no dimer states ( $V_{\text{LJ}}^{(0)}$ ). According to Ref. [3], the scattering hypervolume at  $a = 0$  is related to the curvature  $\tilde{u}_c''$  of the energy per particle of this Bose fluid by

$$D = -3\pi^2 a_\Lambda^2 \lambda^2 r_{\text{vdW}}^2 \frac{1}{\tilde{u}_c''}. \quad (\text{S7})$$

Here  $a_\Lambda$  is a dimensionless parameter that characterizes the zero crossing of  $a$  [3]. From the scattering length of  $V_{\text{LJ}}^{(0)}$ , we find that  $a_\Lambda = 3.82812(5)$  and  $r_{\text{vdW}}/\lambda = 0.858036(1)$  at  $a = 0$ . Since  $\tilde{u}_c'' = -6.547$  [44], Eq. (S7)



gives  $D/r_{\text{vdW}}^4 = 90.02$ . The uncertainty in this prediction is determined by the uncertainty in the value of  $\tilde{u}_c''$ .

## VI. COLLECTIVE MODES

Here we provide more details about the variational method used to obtain the collective mode spectrum at  $a = 0$ , noting that similar calculations for a Gross-

Pitaevskii equation with a cubic nonlinearity have appeared also in Ref. [51]. Beginning from the Gaussian trial wave function [49, 50] given by Eq. (7) of the main text

$$\Psi(x, y, z, t) = A(t) \prod_{\eta=x,y,z} e^{-\frac{(\eta-\eta_0)^2}{2w_\eta^2} + i\eta\alpha_\eta + i\eta^2\beta_\eta}, \quad (\text{S8})$$

we obtain the Lagrangian

$$\begin{aligned} \frac{2L}{N} = & - \left[ \sum_{\eta} \left( \hbar\partial_t\beta_\eta + \frac{2\hbar^2\beta_\eta^2}{m} + \frac{1}{2}m\lambda_\eta^2\omega_{\text{ho}}^2 \right) \times (w_\eta^2 + 2\eta_0^2) + \left( \hbar\partial_t\alpha_\eta + \frac{2\hbar^2\alpha_\eta\beta_\eta}{m} \right) 2\eta_0 + \frac{\hbar^2}{2mw_\eta^2} + \frac{\hbar^2\alpha_\eta^2}{m} \right] \\ & - \frac{N^2\hbar^2 D}{3^{5/2}\pi^3 w_x^2 w_y^2 w_z^2} + i\hbar \left[ \frac{\partial_t A}{A} - \frac{\partial_t A^*}{A^*} \right]. \end{aligned} \quad (\text{S9})$$

From the Euler-Lagrange equations, we find

$$\beta_\eta = m(\partial_t w_\eta)/2\hbar^2 w_\eta, \quad (\text{S10})$$

$$\alpha_\eta = \frac{m}{\hbar} \left( \partial_t \eta_0 - \frac{\eta_0 \partial_t w_\eta}{w_\eta} \right), \quad (\text{S11})$$

$$\partial_t^2 \eta_0 + \lambda_\eta^2 \omega_{\text{ho}}^2 \eta_0 = 0, \quad (\text{S12})$$

$$\partial_\tau^2 v_\eta + \lambda_\eta^2 v_\eta = \frac{1}{v_\eta^3} + \frac{K}{v_\eta(v_x v_y v_z)^2}, \quad (\text{S13})$$

with  $K = 2DN^2/9\sqrt{3}\pi^3 l_{\text{ho}}^4$  and dimensionless scalings  $v_\eta = w_\eta/l_{\text{ho}}$  and  $\tau = \omega_{\text{ho}} t$ . From Eq. (S13), we identify Newton's equations for classical motion in an effective

potential

$$\begin{aligned} U(v_x, v_y, v_z) = & \frac{1}{2}(\lambda_x^2 v_x^2 + \lambda_y^2 v_y^2 + \lambda_z^2 v_z^2) \\ & + \frac{1}{2} \left( \frac{1}{v_x^2} + \frac{1}{v_y^2} + \frac{1}{v_z^2} \right) + \frac{K}{2(v_x v_y v_z)^2}. \end{aligned} \quad (\text{S14})$$

To study the collective mode spectrum, Eq. (S13) must be solved for the equilibrium widths  $v_\eta$ , and then linearized about harmonic perturbations to these equilibrium solutions  $\delta v_\eta e^{-i\omega t}$ . The frequencies  $\omega$  are eigenvalues of the  $3 \times 3$  Hessian matrix  $U_{ij} = \partial^2 U / \partial v_i \partial v_j$

$$\omega_{022}/\omega_{\text{ho}} = \sqrt{U_{11} - U_{12}}, \quad (\text{S15})$$

$$\omega_{100}/\omega_{\text{ho}} = \frac{1}{\sqrt{2}} \sqrt{U_{11} + U_{12} + U_{33} + \sqrt{U_{11}^2 + 2U_{11}U_{12} + U_{12}^2 + 8U_{13}^2 - 2U_{11}U_{33} - 2U_{12}U_{33} + U_{33}^2}}, \quad (\text{S16})$$

$$\omega_{020}/\omega_{\text{ho}} = \frac{1}{\sqrt{2}} \sqrt{U_{11} + U_{12} + U_{33} - \sqrt{U_{11}^2 + 2U_{11}U_{12} + U_{12}^2 + 8U_{13}^2 - 2U_{11}U_{33} - 2U_{12}U_{33} + U_{33}^2}}, \quad (\text{S17})$$

where the indices  $\omega_{nlm}$  indicate the associated principle and angular quantum numbers for a particular mode [49].

Finally, we give analytic results from the variational calculations for a cylindrical trap ( $\lambda_x = \lambda_y = 1$ ). In the limit  $K \ll 1$ , we take  $K = 0$  to obtain the ground state widths  $v_x = v_y = 1$  and  $v_z = 1/\sqrt{\lambda_z}$ , and find the

spectrum

$$\omega_{022}/\omega_{\text{ho}} = 2, \quad (\text{S18})$$

$$\omega_{100}/\omega_{\text{ho}} = \begin{cases} 2\lambda_z & \text{if } \lambda_z \geq 1, \\ 2 & \text{if } \lambda_z < 1, \end{cases} \quad (\text{S19})$$

$$\omega_{020}/\omega_{\text{ho}} = \begin{cases} 2 & \text{if } \lambda_z \geq 1, \\ 2\lambda_z & \text{if } \lambda_z < 1. \end{cases} \quad (\text{S20})$$

In the limit  $K \gg 1$ , we ignore the kinetic dispersion

term to obtain the equilibrium widths  $v = K^{1/8}\lambda_z^{1/4}$  and  $v_z = K^{1/8}\lambda_z^{-3/4}$ , which gives the spectrum

$$\omega_{022}/\omega_{\text{ho}} = \sqrt{2}, \quad (\text{S21})$$

$$\omega_{100}/\omega_{\text{ho}} = \sqrt{3 + 2\lambda_z^2 + \sqrt{9 - 4\lambda_z^2 + 4\lambda_z^4}}, \quad (\text{S22})$$

$$\omega_{020}/\omega_{\text{ho}} = \sqrt{3 + 2\lambda_z^2 - \sqrt{9 - 4\lambda_z^2 + 4\lambda_z^4}}. \quad (\text{S23})$$